Spin pumping damping and magnetic proximity effect in Pd and Pt spin-sink layers

M. Caminale,[1,2,*] A. Ghosh,[2,†] S. Auffret,[2] U. Ebels,[2] K. Ollefs,[3] F. Wilhelm,[4] A. Rogalev,[4] and W. E. Bailey[1,5,‡]

[1]*Fondation Nanosciences, F-38000 Grenoble, France*
[2]*SPINTEC, Université Grenoble Alpes / CEA / CNRS, F-38000 Grenoble, France*
[3]*Fakultät für Physik and Center for Nanointegration (CENIDE), Universität Duisburg-Essen, 47057 Duisburg, Germany*
[4]*European Synchrotron Radiation Facility (ESRF), 38054 Grenoble Cedex, France*
[5]*Department of Applied Physics & Applied Mathematics, Columbia University, New York, New York 10027, USA*

We investigated the spin pumping damping contributed by paramagnetic layers (Pd, Pt) in both direct and indirect contact with ferromagnetic $Ni_{81}Fe_{19}$ films. We find a nearly linear dependence of the interface-related Gilbert damping enhancement $\Delta\alpha$ on the heavy-metal spin-sink layer thicknesses t_N in direct-contact $Ni_{81}Fe_{19}$/(Pd, Pt) junctions, whereas an exponential dependence is observed when $Ni_{81}Fe_{19}$ and (Pd, Pt) are separated by 3 nm Cu. We attribute the quasilinear thickness dependence to the presence of induced moments in Pt, Pd near the interface with $Ni_{81}Fe_{19}$, quantified using x-ray magnetic circular dichroism measurements. Our results show that the scattering of pure spin current is configuration-dependent in these systems and cannot be described by a single characteristic length.

I. INTRODUCTION

As a novel means of conversion between charge currents and spin currents, spin Hall phenomena have recently opened up new possibilities in magnetoelectronics, with potential applications in mesoscale spin torques and electrical manipulation of domain walls [1–9]. However, several aspects of the scattering mechanisms involved in spin current flow across thin films and interfaces are not entirely understood. Fundamental studies of spin current flow in ferromagnet/nonmagnetic-metal (F/N) heterostructures in the form of continuous films have attempted to isolate the contributions of interface roughness, microstructure, and impurities [10–12]. Prototypical systems in this class of studies are $Ni_{81}Fe_{19}$/Pt (Py/Pt) [3,5–7,13–18] and $Ni_{81}Fe_{19}$/Pd (Py/Pd) [8,11,14,16,19,20] bilayers. In these systems, Pt and Pd are employed either as efficient spin sinks or spin/charge current transformers, in spin pumping and spin Hall experiments, respectively. Pd and Pt are metals with high paramagnetic susceptibility and when placed in contact with a ferromagnetic layer (e.g., Py, Ni, Co, or Fe) a finite magnetic moment is induced at the interface by direct exchange coupling [21–24].

The role of the magnetic proximity effect on interface spin transport properties is still under debate. Zhang *et al.* [25] have reported that induced magnetic moments in Pt and Pd films in direct contact with Py correlate strongly reduced spin Hall conductivities. This is ascribed to a spin splitting of the chemical potential and on the energy dependence of the intrinsic spin Hall effect. In standard spin pumping theory [26], possible induced moments in N are supposed to be *a priori* included in calculations of the spin-mixing conductance $g^{\uparrow\downarrow}$ of a F|N interface [27,28], which tends to be insensitive to their presence.

Recent theoretical works, on the other hand, propose generalized spin pumping formalisms including spin flip and spin orbit interaction at the F|N interface, in order to justify discrepancies between experimental and calculated values of mixing conductance [29,30]. At present, it is still an open issue whether and how proximity-induced magnetic moments in F/N junctions are linked to the variety of the spin-transport phenomena reported in the literature [10,17,31].

Here, we present an experimental study of the prototypical heterostructure system Py/(Pd, Pt) and Py/Cu/(Pd, Pt). The objective of our study is to address the role of proximity-induced magnetic moments in spin pumping damping. To this end, we employed two complementary experimental techniques. X-ray magnetic circular dichroism (XMCD) is an element-sensitive technique which allows us to quantify any static proximity-induced magnetic moments in Pt and Pd. Ferromagnetic resonance (FMR) measurements provide indirect information on the spin currents pumped out the Py layer by the precessing magnetization, through the characterization of the Pd, Pt thickness dependence of the interface-related Gilbert damping α. In Fig. 3 (Sec. III B), comparative measurements in Py/Cu/N and Py/N structures show a change of the N-thickness dependence of $\Delta\alpha(t_N)$ from an exponential to a linear-like behavior. A change in $\Delta\alpha(t_N)$ indicates a transformation in the spin scattering mechanism occurring at the interface, ascribed here to the presence of induced moments in directly exchange coupled F/N systems. Theoretical works predicted a deviation from a conventional N-thickness dependence when interface spin-flip scattering is considered in the pumping model [29,30], but no functional form was provided. For Py/N systems, we find that the experimental thickness dependence cannot be described well by standard models [16,26,32], but rather a linear function reproduces the data to a better degree of accuracy, introducing a different characteristic length. We speculate that the spatial extent of spin current absorption in F/N systems shows an inverse proportionality to interfacial exchange coupling energy, obtained from XMCD, as proposed before for spin-polarized, decoupled interfaces in F_1/Cu/F_2 heterostructures [14].

---

*michael.caminale@cea.fr
†Present address: Data Storage Institute, Agency for Science, Technology, and Research (A*STAR), Singapore 138634.
‡web54@columbia.edu

II. EXPERIMENT

The heterostructures were fabricated by dc magnetron sputtering on ion-cleaned Si/SiO$_2$ substrates in the form of *substrate/seed/multilayer/cap* stacks, where a Ta(5 nm)/Cu(5 nm) bilayer was employed as *seed*. Ta/Cu is employed to promote ⟨111⟩ growth in Py and subsequent fcc layers (Pd, Pt), and Ta is known to not affect the damping strongly [17,32,33]. Different stacks were grown as *multilayer* for each measurement.

For FMR measurements, we have *multilayer* = Py(t_F)/N(t_N), Py(t_F)/Cu(3 nm)/N(t_N) with N = Pd, Pt; an Al(3 nm) film, oxidized in air, was used as *cap*. The smallest N-layer thickness t_N deposited is 0.4 nm, the maximum interdiffusion length observed for similar multilayers [34]. Samples with *multilayer* = Py(t_N)/Cu(3 nm) and no sink layer were also fabricated as reference for evaluation of the Gilbert damping enhancement due to the Pd or Pt layer. The t_N-dependence measurements of FMR were taken for Py thicknesses t_F = 5 and 10 nm. Results from the t_F = 10 nm data set are shown in Appendix B. Measurements of the FMR were carried out at fixed frequency ω in the 4–24 GHz range, by means of an in-house apparatus featuring an external magnetic field 0–0.9 T, applied parallel to a coplanar waveguide with a broad center conductor width of 350 μm.

For XMCD measurements, given the low x-ray absorption cross section presented by Pt and Pd absorption edges, a special set of samples was prepared, consisting of Y repeats—with Y = 20 or 15, as specified in the figure captions of the data presented—per structure in order to obtain sufficiently high signal-to-noise ratio. In this case, we have *multilayer* = [Py(5 nm)/Cu(0, 0.5, 1, 3 nm)/N/Cu(0, 0.5, 1, 3 nm)]$_Y$, with N = Pd(2.5 nm) and Pt(1 nm); Py(5 nm)/Cu(5 nm)/Al(3 nm) was deposited as *cap*. The Pt and Pd thicknesses were chosen to yield a damping enhancement equal about to half of the respective saturation value (as will be shown later), i.e., a thicknesses for which the F/N interface is formed but the damping enhancement is still increasing. XMCD experiments were carried out at the Circular Polarization Beamline ID-12 of the European Synchrotron Radiation Facility (ESRF) [35]. Measurements were taken in total fluorescence yield detection mode, at grazing incidence of 10°, with either left or right circular helicity of the photon beam, switching a 0.9 T static magnetic field at each photon energy value (further details on the method are in Ref. [22]). No correction for self-absorption effects is needed; however XMCD spectra measured at the L$_{2,3}$ edges of Pd have to be corrected for incomplete circular polarization of monochromatic x-rays, 12% and 22% at L$_3$ and L$_2$, respectively. The circular polarization rate is in excess of 95% at the L$_{2,3}$ edges of Pt.

III. RESULTS AND ANALYSIS

In order to study how the proximity-induced magnetic moments affect the absorption of spin currents through interfaces, the static moment induced in Pt, Pd layers in direct contact with ferromagnetic Py is characterized first, by means of XMCD. The value of the induced moment extracted for the two Py/N systems is used to estimate the interfacial exchange energy acting on the two paramagnets (as described in Sec. III A). Afterwards, the dynamic response of the magnetization is

addressed by FMR measurements in Py/N (direct contact) and Py/Cu/N (indirect contact) heterostructures. From FMR measurements carried out on both configurations as a function of N thickness, the damping enhancement due to the presence of the spin-sink layers Pt and Pd is obtained from the frequency dependence of the FMR linewidth. The relation between the static induced moment and the spin pumping damping is discussed by comparing the results of the direct- and indirect-contact systems.

A. XMCD: Probing the induced magnetic moment

In Fig. 1 we show x-ray absorption (XAS) and magnetic circular dichroism (XMCD) spectra at the L$_{2,3}$ edges of Pt (top panel) and Pd (bottom panel), taken on [Py(5 nm)/Pt(1 nm)]$_{20}$ and [Py(5 nm)/Pd(2.5 nm)]$_{20}$, respectively. Rather intense XMCD signals have been detected at both Pt and Pd L$_{2,3}$ edges, showing unambiguously that a strong magnetic moment is induced by direct exchange coupling at the Py|N interface. The static induced moment is expected to be ferromagnetically coupled with the magnetization in Py [21]. From the integrals of XMCD spectra, the induced magnetic moment on the Pt, Pd sites is determined by applying the sum rules as in Ref. [22] (and references therein). In [Py/Pd(2.5 nm)]$_{20}$, Pd atoms bear a moment of 0.12 μ_B/at, averaged over the full Pd film thickness, with an orbital-to-spin ratio m_L/m_S = 0.05. In [Py/Pt(1 nm)]$_{20}$, a magnetic moment 0.27 μ_B/at is found on Pt, comparable to that reported in Ni/Pt epitaxial multilayers [23], with a relatively high orbital character m_L/m_S = 0.18, as compared with the Pd induced moment. The large difference
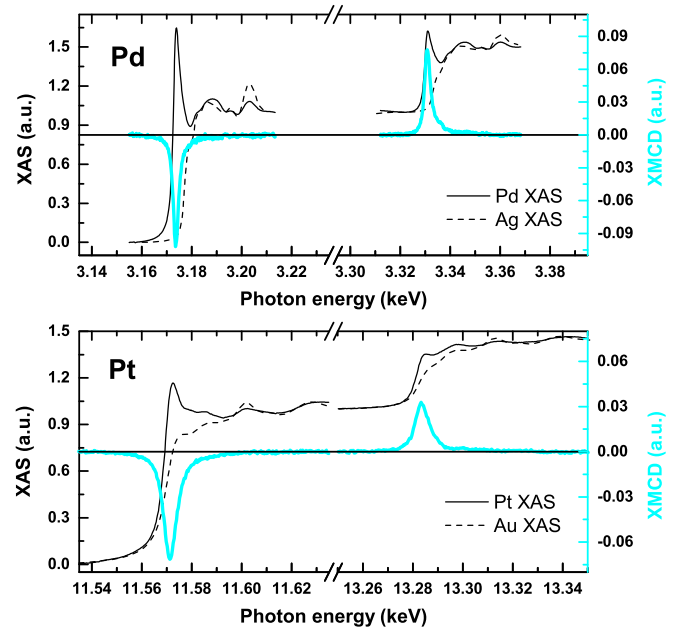

FIG. 1. X-ray absorption (XAS, left axis) and magnetic circular dichroism (XMCD, right axis) spectra at the L edges of Pd (top panel) and Pt (bottom panel) for [Py(5 nm)/Pt(1 nm)]$_{20}$ and [Py(5 nm)/Pd(2.5 nm)]$_{20}$ multilayers. The dashed traces represent XAS spectra at L edge of Ag and Au used as background of Pd and Pt, respectively, to extract the values of induced magnetic moment reported in Table I.
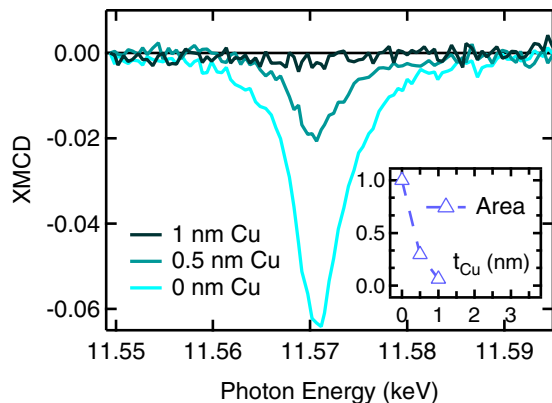
FIG. 2. XMCD spectra at the L_3 edge of Pt for [Py(5 nm)/Cu(t_{Cu})/Pt(1 nm)]$_{15}$, with $t_{Cu} = 0$, 0.5, and 1 nm. Inset: The area of the L_3 XMCD peak is plotted as a function of Cu thickness.

in volume-averaged induced moment per atom comes from the different film thickness, hence volume, for Pt and Pd. Assuming that the induced magnetic moment is confined to the first atomic layers at the interface with Py [23,24], one could estimate $0.32\,\mu_B$/at for Pd and $0.30\,\mu_B$/at for Pt [36].

When a 3 nm thick Cu interlayer is introduced between Py and N, a two orders of magnitude smaller magnetic moment ($0.0036\,\mu_B$/at) was found for 2.5 nm Pd [22], while Pt showed an XMCD signal of the order of the experimental sensitivity—$\sim 0.5 \times 10^{-3}\,\mu_B$/at (see spectra in Fig. 7, Appendix A). In Fig. 2 XMCD spectra at the L_3 edge of Pt are shown for Cu interlayer thicknesses 0, 0.5, and 1 nm. For 0.5 nm Cu the integral of XMCD signal at the L_3 edge shrinks to 30%, while for 1 nm it is reduced to zero within experimental error. This result could be explained either by a 3d growth of the Cu layer, allowing a fraction of the Pt layer to be in direct contact with Py for Cu coverages of 0.5 nm, or by diffusion of magnetic Ni atoms in Cu on a scale shorter than 1 nm. The film then becomes continuous, and at 1 nm coverage, no direct exchange coupling takes place between Py and Pt layers. For FMR measurements presented in the following section, a 3 nm thick Cu interlayer is employed, reducing also any possible indirect exchange coupling.

From the values of induced moments in Pd and Pt, we can make a step forward and estimate the interfacial exchange coupling energies for the two cases. Equating interatomic exchange energy J_{ex} and Zeeman energy for an interface paramagnetic atom, we have (see Appendix C 1 for the derivation)

$$J_{ex} = \frac{1}{2}\frac{\langle M \rangle}{\mu_B N_0 S}\frac{t_N}{t_i}, \qquad (1)$$

where $\langle M \rangle$ is the thickness-averaged paramagnetic moment, N_0 is the single-spin density of states (in eV^{-1} at^{-1}), S is the Stoner factor, and $t_i = 2(a/\sqrt{3})$ is the polarized interface-layer thickness [36]. The $\frac{1}{2}$ factor accounts for the fact that in XMCD measurements the N layer has both interfaces in contact with F. Under the simplifying assumption that all the magnetic moment is confined to the interface N layer and assuming experimental bulk susceptibility parameters for

χ_v, we obtain $J_{ex}^{Pd} = 42$ meV for Pd and $J_{ex}^{Pt} = 109$ meV for Pt (results and properties are summarized in Table I). Here the difference in estimated J_{ex}, despite roughly equal M_i, comes from the larger Stoner factor S for Pd. A stronger interfacial exchange energy in Pt denotes a stronger orbital hybridization, yielding possibly a higher orbital character of the interfacial magnetic moment in the ferromagnetic Py counterpart [21]. For comparison, we consider the interatomic exchange parameters J_{ex} in ferromagnetic Py and Co, investigated in Ref. [14]. J_{ex} is estimated from the respective Curie temperatures T_C, through $J_{ex} \simeq 6k_B T_C/(m/\mu_B)^2$, where m is the atomic moment in μ_B/at (see Appendix C 2). Experimental Curie temperatures of 870 K and 1388 K give $J_{ex}^{Co} = 293$ meV for Co and $J_{ex}^{Py} = 393$ meV for Py, which are of the same order of the value calculated for Pt (details of calculation in Appendix C 2).

In the following, the effect of these static induced moments on the spin pumping damping of the heterostructures characterized will be discussed.

B. FMR: Damping enhancement

The main result of our work is now shown in Fig. 3. In Fig. 3 the damping enhancement $\Delta\alpha$ is plotted as a function of the spin-sink layer thickness t_N, for Py/Pd, Py/Cu/Pd [panel (a)] and Py/Pt, Py/Cu/Pt [panel (b)]. The enhancement $\Delta\alpha$ is compared with the damping α of a reference structure Py(5 nm)/Cu, excluding the sink layer N. Each value of α results from established analysis of the linewidth of 11 FMR traces [13,14], employing a g factor equal to 2.09 as a constant fit parameter for all samples.

In Py/Cu/N systems (Fig. 3, green square markers), $\Delta\alpha$ rises with increasing t_N thickness to similar saturation values $\Delta\alpha_0 = 0.0028$, 0.0031 for Pd and Pt, but reached on different length scales, given the different characteristic spin relaxation lengths of the two materials. From the saturation value, an effective mixing conductance $g_{eff}^{\uparrow\downarrow}(\text{Py}|\text{Cu}/\text{N}) = 7.5$–$8.3$ nm^{-2} is deduced in the framework of the standard spin pumping picture [13,17,19], with Py saturation magnetization $\mu_0 M_s = 1.04$ T. The fact that the spin-mixing conductance is not material-dependent indicates that similar Cu|N interfaces are formed. The thickness dependence is well described by the *exponential* function [14,20]

$$\Delta\alpha(t_N) = \Delta\alpha_0\left[1 - \exp\left(-2t_N/\lambda_\alpha^N\right)\right] \qquad (2)$$

as shown by the fit in Figs. 3(a) and 3(b) (continuous line). As a result, exponential decay lengths $\lambda_\alpha^{Pt} = 1.8$ nm and $\lambda_\alpha^{Pd} = 5.8$ nm are obtained for Pt and Pd, respectively.

When the Pt, Pd spin-sink layers come into direct contact with the ferromagnetic Py, the damping enhancement $\Delta\alpha(t_N)$ changes dramatically. In Py/N systems [Figs. 3(a) and 3(b), triangle markers], the damping saturation values become $\Delta\alpha_0^{Pt} = 0.0119$ and $\Delta\alpha_0^{Pd} = 0.0054$ for Pt and Pd, respectively, a factor ~ 2 and ~ 4 larger as compared to Py/Cu/N. Within the spin pumping description, a larger damping enhancement implies a larger spin-current density pumped out of the ferromagnet across the interface and depolarized in the sink.

In Py/N heterostructures, because of the magnetic proximity effect, few atomic layers in N are ferromagnetically polarized, with a magnetic moment decaying with distance

TABLE I. Spin-sink layer N properties in Py/N heterostructures: experimental molar susceptibility χ_{mol} at 20 °C; density of states N_0 calculated from tabulated χ_{mol}; Stoner parameter S from Ref. [37]; bulk lattice parameter a; layer thicknesses t_N; volume-averaged induced magnetic moment $\langle M \rangle$ from XMCD measurement in Fig. 1; interface magnetic moment M_i [36]; Py|N interfacial exchange energy per interface atom J_{ex} [Eq. (1)].

N	χ_{mol} [37] (cm^3/mol) (10^{-4})	S [37]	N_0 (1/eV · at)	a_{bulk} (nm)	t_N (nm)	$\langle M \rangle$ (μ_B/at)	M_i (μ_B/at)	J_{ex} (meV)
Pd	5.5 ± 0.2	9.3	0.83 ± 0.03	0.389	2.5	0.116	0.32	42
Pt	1.96 ± 0.1	3.7	0.74 ± 0.04	0.392	1.0	0.27	0.30	109

from the Py|N interface. The higher value of damping at saturation might therefore be interpreted as the result of a magnetic bilayer structure, with a thin ferromagnetic N characterized by high damping α_{high}^N coupled to a low damping α_{low}^F ferromagnetic Py [38]. To investigate whether damping is of bilayer type or truly interfacial, in Fig. 4 we show the t_F thickness dependence of the damping enhancement $\Delta\alpha$, for a Py(t_F)/Pt(4 nm) series of samples. The power law thickness dependence adheres very closely to t_F^{-1}, as shown in the logarithmic plot. The assumption of composite damping for synchronous precession, as $\Delta\alpha(t_1) = (\alpha_1 t_1 + \alpha_2 t_2)/(t_1 + t_2)$, shown here for $t_2 = 0.25$ and 1.0 nm, cannot follow an inverse thickness dependence over the decade of $\Delta\alpha$ observed. Damping is therefore observed to have a purely interfacial character.

In this case, the mixing conductances calculated from the saturation values are $g_{eff}^{\uparrow\downarrow}(Py|Pd) = 14\,\text{nm}^{-2}$ and $g_{eff}^{\uparrow\downarrow}(Py|Pt) = 32\,\text{nm}^{-2}$. From *ab initio* calculations within a standard spin pumping formalism in diffusive films [10,29], $g_{eff}^{\uparrow\downarrow}(Py|Pd) = 23\,\text{nm}^{-2}$ for Pd and $g_{eff}^{\uparrow\downarrow}(Py|Pt) = 22\,\text{nm}^{-2}$ for Pt are found. Theoretical spin mixing conductance from a standard picture

does reproduce the experimental order of magnitude, but it misses the 2.3 factor between the Py|Pt and Py|Pd interfaces. Beyond a standard pumping picture, Liu and coworkers [29] introduce spin-flipping scattering at the interface and calculate from first principles, for ideal interfaces in finite diffusive films: $g_{eff}^{\uparrow\downarrow}(Py|Pd) = 15\,\text{nm}^{-2}$, in excellent agreement with the experimental value here reported for Pd (Table II), and $g_{eff}^{\uparrow\downarrow}(Py|Pt) = 25\,\text{nm}^{-2}$. Zhang *et al.* [10] suggest an increase up to 25% of the mixing conductance can be obtained by introducing magnetic layers on the Pt side. The results here reported support the emerging idea that a generalized model of spin pumping including spin-orbit coupling and induced magnetic moments at F|N interfaces may be required to describe the response of heterostructures involving heavy elements.

The saturation value of damping enhancement $\Delta\alpha_0$ as a function of the Cu interlayer thickness is shown in Fig. 5 to follow the same trend of the XMCD signal (dashed line), extracted from Fig. 2. Indeed, it is found that the augmented $\Delta\alpha_0$ in Py/N junctions is drastically reduced by the insertion of 0.5 nm Cu at the Py|N interface [17], and the saturation of
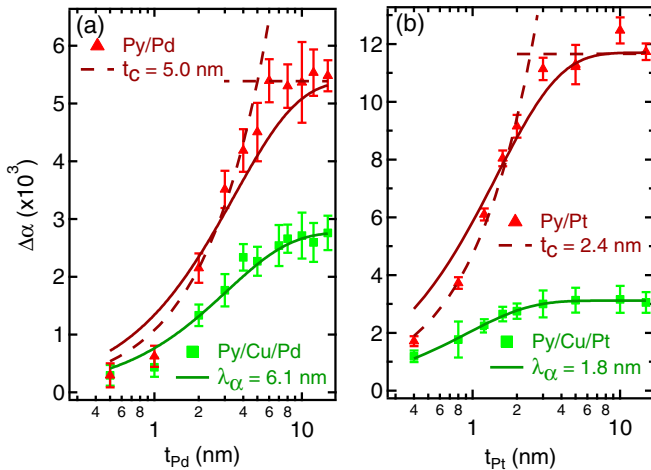
FIG. 3. Damping enhancement $\Delta\alpha$, due to pumped spin current absorption, as a function of thickness t_N for Py(5 nm)/N and Py(5 nm)/Cu(3 nm)/N heterostructures, with N = Pd(t_N) (a), Pt(t_N) (b). Solid lines result from a fit with exponential function [Eq. (2)] with decay length λ_α. Dashed lines represent instead a linear-cutoff behavior [Eq. (3)] for $t_N < t_c$. Error bars show 95% confidence intervals. Notice in panels (a) and (b) that the thickness axis is logarithmic.
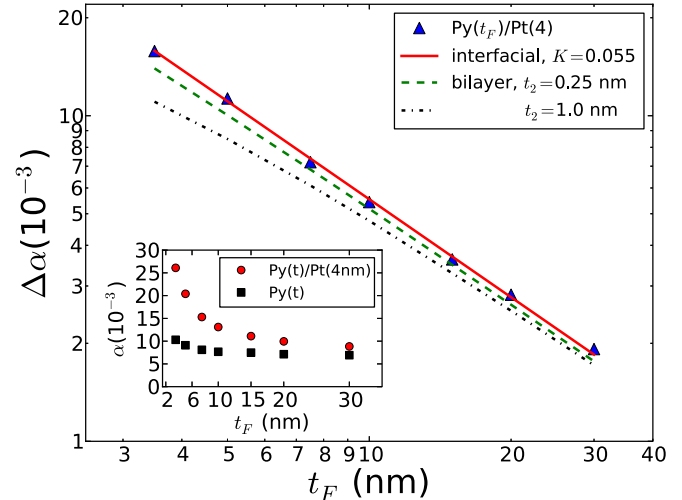
FIG. 4. Logarithmic plot of the damping enhancement $\Delta\alpha$ (triangle markers) as a function of the Py layer thickness t_F, in Py(t_F)/Pt(4 nm). Solid and dashed lines represent, respectively, fits according to the spin pumping (*interfacial*) model $\Delta\alpha = K t_F^{-1}$ and to a $\alpha^{low}(t_F)/\alpha^{high}(t_2)$ *bilayer* model, with $t_2 = 0.25, 1.0$ nm. Inset: Gilbert damping α for Py(t_F) (square markers) and Py(t_F)/Pt(4 nm) (round markers).

TABLE II. Mixing conductance values extracted from the damping enhancement $\Delta\alpha$ at saturation in Fig. 3, and respective length scales (see text for details).

N	$g_{\mathrm{eff}}^{\uparrow\downarrow}$(Py|Cu/N) (nm^{-2})	λ_α (nm)	$g_{\mathrm{eff}}^{\uparrow\downarrow}$(Py|N) (nm^{-2})	t_c (nm)
Pd	7.5 ± 0.2	6.1 ± 0.6	14 ± 1	5.0 ± 0.4
Pt	8.3 ± 0.2	1.8 ± 0.3	32 ± 1	2.4 ± 0.2

the Py/Cu/N configuration is already reached for 1 nm of the Cu interlayer. As soon as a continuous interlayer is formed and no magnetic moment is induced in N, $\Delta\alpha_0$ is substantially constant with increasing Cu thickness.

The N-thickness dependence of $\Delta\alpha(t_N)$ in Py/N systems before saturation is addressed in the following. In contrast to the Py/Cu/N case, the thickness dependence of $\Delta\alpha$ is no longer well described by an exponential saturation, as a fit to Eq. (2), with exponential decay length as the only free fit parameter, fails to reproduce the increase of $\Delta\alpha$ towards saturation [solid lines in Figs. 3(a) and 3(b)]. More rigorous fitting functions employed in spin pumping experiments, within standard spin transport theory [16,26,32], also cannot reproduce the experimental data as well (see Appendix B). It is worth mentioning that the same change of trend between the two configurations was observed for the same stacks with a 10 nm thick Py layer (data shown in Appendix B, Fig. 8). A change of the functional dependence of $\Delta\alpha$ on t_N reflects a change in the spin-depolarization processes undergone by the pumped spin current, as shown for instance in Ref. [30], when interfacial spin-orbit coupling is introduced in the spin pumping formalism. Experimentally, a *linear* thickness dependence with sharp cutoff has been shown to characterize spin-current absorption in spin-sink layers exhibiting ferromagnetic order at the interface, as reported for F_1/Cu/$F_2(t_{F_2})$ junctions with F = Py, Co, CoFeB [14]. Given the presence of ferromagnetic order in N at the interface of F/N structures, the data are tentatively fitted with a linear function

$$\Delta\alpha = \Delta\alpha_0 t_N / t_c^N. \tag{3}$$

This linear function better reproduces the sharp rise of $\Delta\alpha$ [dashed lines in Figs. 3(a) and 3(b)] and gives cutoff thick-
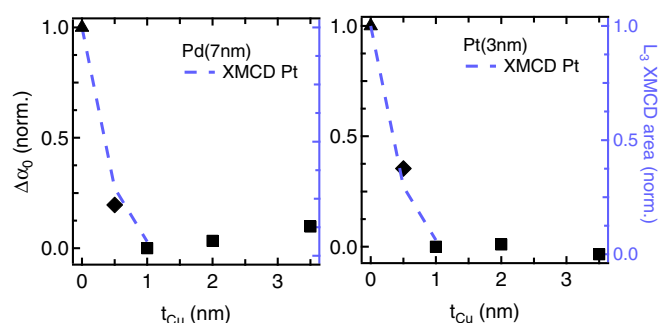

FIG. 5. Damping enhancement $\Delta\alpha_0$ (left axis, normalized as $\Delta\alpha_0(t_{Cu}) \rightarrow [\Delta\alpha_0(t_{Cu}) - \Delta\alpha_0(1\,nm)]/[\Delta\alpha_0(0\,nm) - \Delta\alpha_0(1\,nm)]$), due to spin pumping, as a function of interlayer thickness t_{Cu} for Py(5 nm)/Cu(t_{Cu})/N heterostructures, with N = Pd(7 nm), N = Pt(3 nm). The dashed line represents the XMCD signal (right axis) reported from inset in Fig. 2.
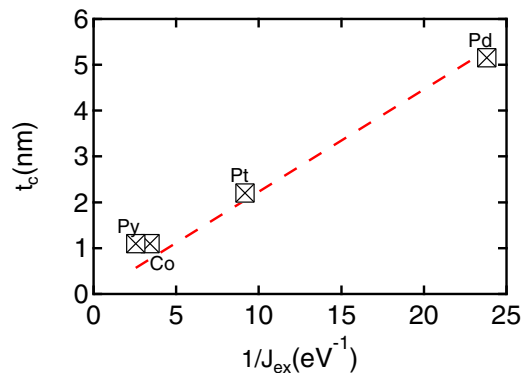

FIG. 6. Effect of direct exchange strength on length scale of spin current absorption. Cutoff thickness t_c extracted from the $\Delta\alpha(t_N)$ data in Fig. 3 as a function of reciprocal interfacial exchange energy $1/J_{ex}$ extracted from XMCD in Fig. 1. Labels are given in terms of J_{ex}. The Co and Py points are from Ref. [14].

nesses $t_c^{Pd} = 5.0 \pm 0.3$ nm and $t_c^{Pt} = 2.4 \pm 0.2$ nm for Pd and Pt, respectively. The linearization is ascribed to the presence of ferromagnetic order in the paramagnetic Pd, Pt spin-sink layers at the interface with the ferromagnetic Py. The linear trend extends beyond the thickness for which a continuous layer is already formed (less than 1 nm), and, especially for Pd, far beyond the distance within the nonuniform, induced moment is confined (up to 0.9 nm [24]). In Ref. [14], the cutoff t_c in F/Cu/F heterostructures is proposed to be on the order of the transverse spin coherence length λ_J in ferromagnetically ordered layers. λ_J can be expressed in terms of the exchange splitting energy J_{ex},

$$\lambda_J = \frac{h v_g}{2 J_{ex}}, \tag{4}$$

where v_g is the electronic group velocity at the Fermi level. This form, found from hot-electron Mott polarimetry [1], is expressed equivalently for free electrons as $\pi/|k^\uparrow - k^\downarrow|$, which is a scaling length for geometrical dephasing in spin momentum transfer [2]. Electrons which enter the spin-sink at E_F do so at a distribution of angles with respect to the interface normal, traverse a distribution of path lengths, and precess by different angles (from minority to majority or vice versa), before being reflected back into the pumping ferromagnet. For a constant v_g, it is therefore predicted that t_c is inversely proportional to the exchange energy J_{ex}.

In Fig. 6 we plot the dependence of the cutoff thickness t_c^N upon the inverse of the estimated exchange energy J_{ex} (Table I), as extracted from the XMCD measurements. A proportionality is roughly verified, as proposed for the transverse spin coherence length across spin-polarized interfaces. Under the simplistic assumption that $t_c = \lambda_J$, from the slope of the line we extract a Fermi velocity of $\sim 0.1 \times 10^6$ m/s [Eq. (4)], of the order of magnitude expected for the materials considered [39,40]. These data show that, up to a certain extent, the length scale for spin-current scattering shares a common physical origin in ferromagnetic layers and paramagnetic heavy metals, such as Pd and Pt, under the influence of the magnetic proximity effect. This unexpected result is observed in spite of the fact that F_1/Cu/F_2 and F/N systems present fundamental

differences. In F/N structures, the induced moment in N is expected to be directly exchange coupled with the ferromagnetic counterpart. In $F_1/Cu/F_2$, the magnetic moment in F_2 (off-resonance) is only weakly coupled with the precession occurring in F_1 (in-resonance), through spin-orbit torque and possible RKKY interaction. Magnetization dynamics in N might therefore be expected with its own pumped spin current, though, to the best of our knowledge, no experimental evidence of a dynamic response of proximity-induced moments has been reported so far. From these considerations and the experimental findings, counterintuitively the proximity-induced magnetic moments appear not to be involved in the production of spin current, but rather to contribute exclusively with an additional spin-depolarization mechanism at the interface.

IV. CONCLUSIONS

We have investigated the effect of induced magnetic moments in heavy metals at Py/Pt and Py/Pd interfaces on the absorption of pumped spin currents, by analyzing ferromagnetic resonance spectra with varying Pt, Pd thicknesses. Static, proximity-induced magnetic moments amount to $\sim$0.3 μ_B/atom in both Pd and Pt, at the interface with Py, as deduced from XMCD measurements taken at the $L_{2,3}$ edges. We have shown that when the proximity-induced moment in Pt and Pd is present, an onset of a linear-like thickness dependence of the damping is observed, in contrast with an exponential trend shown by Py/Cu/Pd and Py/Cu/Pt systems, for which no induced moment is measured. These results point to the presence of an additional spin-flip process occurring at the interface and to a change of the character of spin current absorption in the ultrathin Pd and Pt paramagnets because of the interfacial spin polarization. The range of linear increase is proposed to be inversely proportional to the interfacial exchange energy in Py/Pt and Py/Pd, inferred from XMCD data.

APPENDIX A: XMCD—Pt

In Fig. 7 we report the XMCD spectra taken at the L edges of Pt on the [Py(5 nm)/Cu(t_{Cu})/Pt(1 nm)]$_{20}$ multilayer, with $t_{Cu} = 0, 3$ nm. The presence of the 3 nm thick Cu interlayer suppresses any proximity-induced moment in Pt. The signal, at the margin of detectability, is ascribed to the paramagnetic response of the Pt film in 0.6 T magnetic field and perhaps RKKY coupling from the Py layers, at room temperature.

APPENDIX B: N-THICKNESS DEPENDENCE

In order to confirm the results presented in the paper, additional sample series with thicker Py layer were fabricated and measured. The experimental results for the 10 nm thick
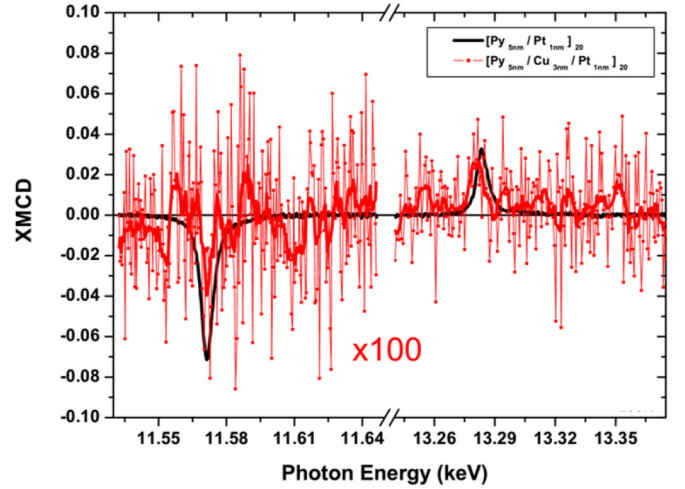

FIG. 7. X-ray absorption magnetic circular dichroism (XMCD) spectra at $L_{3,2}$ absorption edges of Pt for [Py(5 nm)/Pt(1 nm)]$_{20}$ (black solid line) and [Py(5 nm)/Cu(3 nm)/Pt(1 nm)]$_{20}$ (red markers; enhanced by a factor 100) multilayers.

Py layer are shown in Figs. 8 and 9 for Pd and Pt, respectively. We have presented the data here, rather than including them with the other plots in Fig. 3, to keep the figures from being overcrowded. As expected when doubling the ferromagnet thickness, the saturation values $\Delta\alpha_0$ are about half of those measured for 5 nm Py (Fig. 3). Confirming the data presented in the paper, we again observe a change of thickness dependence of $\Delta\alpha(t_N)$, from *exponential* for Py/Cu/N [solid lines; Eq. (2), $\lambda_\alpha = 4.8$ nm and 1.4 nm for Pd and Pt, respectively] to *linear*-like for Py/N [dashed lines; Eq. (3), $t_c = 5.3$ nm and 2 nm for Pd and Pt, respectively].

Here we have also considered some alternate fitting forms based on the standard theory of diffusive spin transport [16,26,32], describing the dependence of $\Delta\alpha$ as

$$\Delta\alpha = \frac{\gamma\hbar}{4\pi M_s t_{FM}} \frac{g^{\uparrow\downarrow}}{1 + \frac{g^{\uparrow\downarrow}}{g_{ext}}} \quad (B1)$$

with the g_{ext} functional form determined by the number and properties of the adjacent metallic layers—either N or Cu/N in our case (Eq. (7) in Ref. [16], and Eq. (6) in Ref. [32]):

$$g_{ext}^{N} = g_N \tanh\left(t_N/\lambda_{sd}^{N}\right), \quad (B2a)$$

$$g_{ext}^{Cu/N} = g_{Cu} \frac{g_{Cu} \coth\left(t_N/\lambda_{sd}^{N}\right) + g_N \coth\left(t_{Cu}/\lambda_{sd}^{Cu}\right)}{g_{Cu} \coth\left(t_N/\lambda_{sd}^{N}\right) \coth\left(t_{Cu}/\lambda_{sd}^{Cu}\right) + g_N}, \quad (B2b)$$

where $g_x = \sigma_x/\lambda_{sd}^{x}$, σ_x, and λ_{sd}^{x} are the electrical conductivity and spin diffusion length of the nonmagnetic layer x. For the thin Cu layer, we used a resistivity $\rho_{Cu} = 1 \times 10^{-7}$ Ωm and a spin diffusion length $\lambda_{sd}^{Cu} = 170$ nm [32]. For the Pt and Pd layers, two fitting models in which the conductivity of the films is either constant or thickness-dependent are considered, as recently proposed by Boone and coworkers [16]. The values of conductivity, as taken directly from Ref. [16], will influence the spin diffusion length λ_{sd}^{N} and spin-mixing conductance $g^{\uparrow\downarrow}$ resulting from the fit, but will not affect the conclusions drawn

FIG. 8. Damping enhancement $\Delta\alpha$, due to pumped spin current absorption, as a function of thickness t_{Pd} for Py(10 nm)/Pd and Py(10 nm)/Cu(3 nm)/Pd heterostructures. Solid lines result from a fit with exponential function [Eq. (2)] with decay λ_α. Dashed lines represents instead a linear-cutoff behavior [Eq. (3)] for $t_{Pd} < t_c$. Short-dashed and point-dashed traces are fitted to the data, employing equations from standard spin transport theory (see text for details) [16,32]. In the bottom panel, $\Delta\alpha$ is plotted in linear scale for completeness.
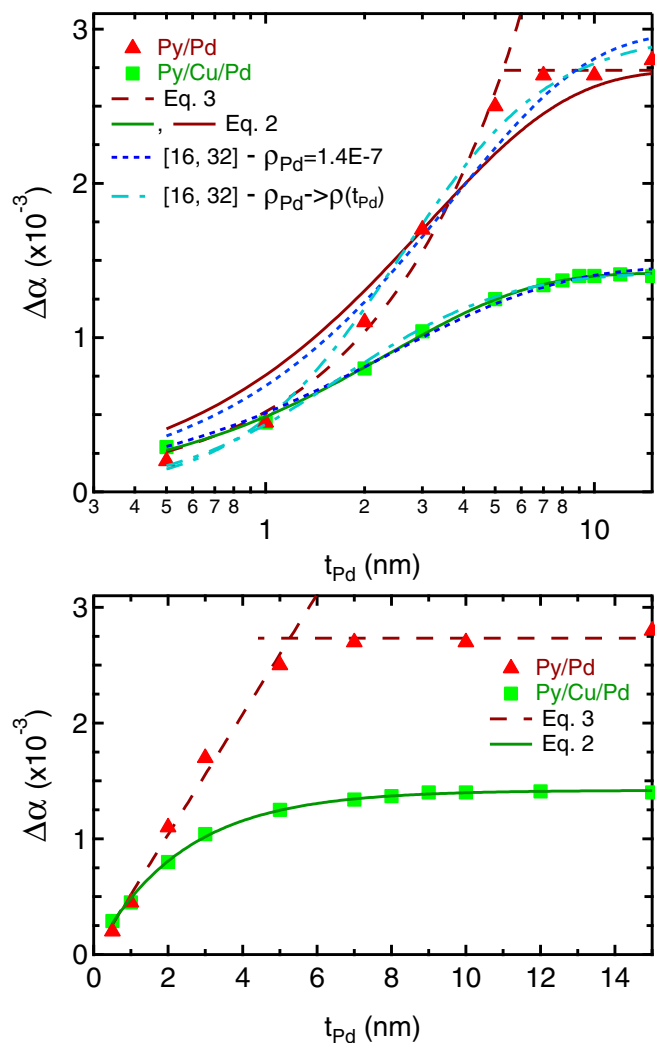
FIG. 9. Damping enhancement $\Delta\alpha$, due to pumped spin current absorption, as a function of thickness t_{Pt} for Py(10 nm)/Pt and Py(10 nm)/Cu(3 nm)/Pt heterostructures. Solid lines result from a fit with exponential function [Eq. (2)] with decay λ_α. Dashed lines represents instead a linear-cutoff behavior [Eq. (3)] for $t_{Pt} < t_c$. Short-dashed and point-dashed traces are fitted to the data, employing equations from standard spin transport theory (see text for details) [16,32]. In the bottom panel, $\Delta\alpha$ is plotted in linear scale for completeness.

about the overall trend. When a constant resistivity is used (short-dashed, blue lines), the model basically corresponds to the simple exponential function in Eq. (2). It nicely reproduces the data in the indirect-contact case (Py/Cu/N) for both Pd (Fig. 8) and Pt (Fig. 9), but it fails to fit the direct-contact (Py/N) configuration. When a thickness-dependent resistivity of the form $\rho_N = \rho_N^b + \rho_N^s / t_N$ is used (point-dashed, cyan lines) [16], in Py/Cu/N systems, no significant difference with the other functions is observed for Pt, while for Pd a deviation from experimental trend is observed below 1.5 nm. In Py/N systems, the fit better describes the rise at thicknesses shorter than the characteristic relaxation length, while it deviates from the data around the saturation range. It is worth mentioning that inserting a fictitious layer in between Py and Pt, Pd to account
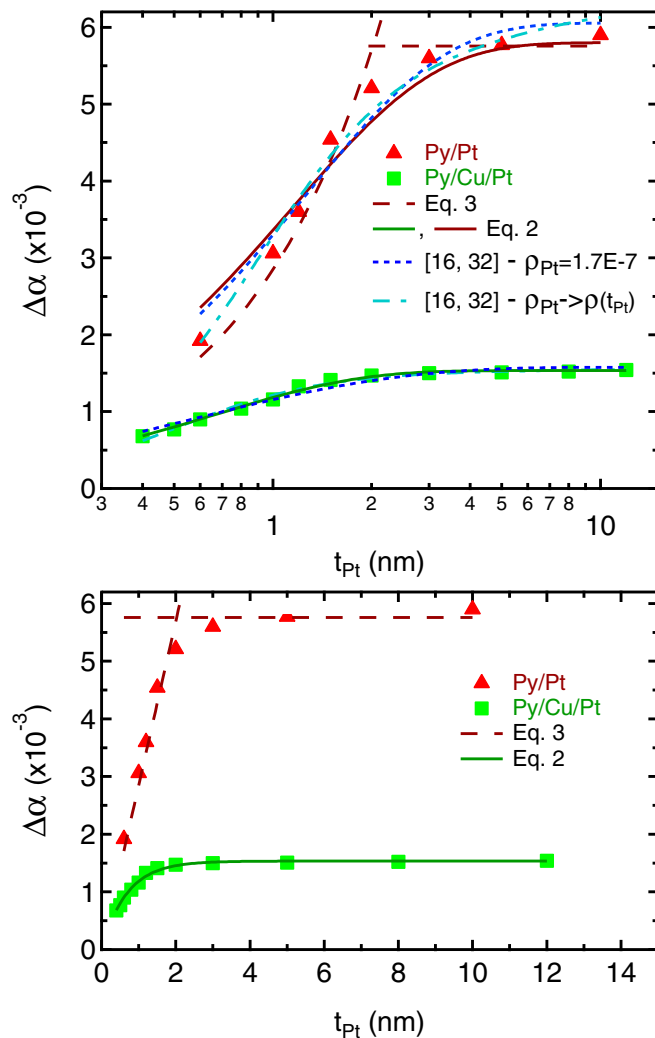
for an additional interfacial spin-flip δ (as in Ref. [16]) did not lead to any improvement in the fit result.

Models from standard spin transport theory cannot satisfactorily describe the experimental data for the direct-contact Py/N systems. For this reason a different mechanism for the spin-depolarization processes has been proposed, considering the presence of induced magnetic moments in N in contact with the ferromagnetic layer.

APPENDIX C: INTERFACIAL INTERATOMIC EXCHANGE

1. Paramagnets

We will show estimates for exchange energy based on XMCD-measured moments in [Py/(Pt, Pd)]$_{repeat}$ superlattices. Calculations of susceptibility are validated against

experimental data for Pd and Pt. Bulk susceptibilities will be used to infer interfacial exchange parameters J_{ex}^i.

Pauli susceptibility. For an itinerant electron system characterized by a density of states at the Fermi energy N_0, if an energy ΔE splits the spin-up and spin-down electrons, the magnetization resulting from the (single-spin) exchange energy ΔE is

$$M = \mu_B(N^\uparrow - N^\downarrow) = 2\mu_B N_0 S \Delta E, \qquad (C1)$$

where N_0 is the density of states in number/eV/at, S is the Stoner parameter, and $2\Delta E$ is the exchange *splitting* in eV. Moments are then given in μ_B/at. Solving for ΔE,

$$\Delta E = \frac{M}{2\mu_B N_0 S}. \qquad (C2)$$

If the exchange splitting is generated through the application of a magnetic field, $\Delta E = \mu_B H$,

$$\mu_B H = \frac{M}{2\mu_B N_0 S}, \qquad (C3)$$

and the dimensionless volume magnetic susceptibility can be expressed

$$\chi_v \equiv \frac{M}{H} = 2\mu_B^2 N_0 S. \qquad (C4)$$

In this expression, the prefactor can be evaluated through

$$\mu_B^2 = 59.218 \text{ eV\AA}^3, \qquad (C5)$$

so with $N_0[=]$/eV/at, χ_v takes units of volume per atom, and is then also called an atomic susceptibility, in cm^3/at, as printed in Ref. [37].

Molar susceptiblity. Experimental values are tabulated as molar susceptibilities. The atomic susceptibility χ_v can be contrasted with the mass susceptibility χ_m and molar susceptibility χ_{mol},

$$\chi_{\text{mass}} = \frac{\chi_v}{\rho}, \quad \chi_{\text{mol}} = \frac{\text{ATWT}}{\rho}\chi_v, \qquad (C6)$$

where ATWT is the atomic weight (g/mol) and ρ is the density (g/cm^3). These have units of $\chi_{\text{mass}}[=]$cm^3/g and $\chi_{\text{mol}}[=]$cm^3/mol. The molar susceptibility χ_{mol} is then

$$\chi_{\text{mol}} = 2\mu_B^2 N_0 N_A S \qquad (C7)$$

in cm^3/mol, where μ_B is the Bohr magneton, and

$$2N_0 S = \frac{\chi_{\text{mol}}}{N_A \mu_B^2}. \qquad (C8)$$

Equation (C8) provides a convenient method to estimate experimental unknowns, the density of states N_0 and Stoner parameter S, from measurements of χ_{mol}.

Example. For Pd, the low-temperature measurement (different from the room-temperature measurement in Table I) is $\chi_{\text{mol}} \sim 7.0 \times 10^{-4}$ cm^3/mol. In the denominator, $(N_A \mu_B^2) = 2.622 \times 10^{-6}$ Ry · cm^3/mol, The value $2N_0 S$ consistent with the experiment is 266/(Ry at) or 19.6/(eV at). For the tabulated measurement of $S = 9.3$, the inferred density of states is then $N_0 = 1.05$/eV/at.

Interfacial exchange. We can assume that the Zeeman energy per interface atom is equal to its exchange energy, through the Heisenberg form

$$\frac{M_p^2}{\chi_v} V_{at} = 2J_{ex}^i s_f s_p, \qquad (C9)$$

where M_p is the magnetization of the paramagnet, with the atomic moment of the paramagnet m_p in terms of its per-atom spin s_p,

$$M_p = \frac{m_p}{V_{at}}, \quad m_p = 2\mu_B s_p. \qquad (C10)$$

V_{at} is the volume of the paramagnetic site, $s_{f,p}$ are the per-atom spin numbers for the ferromagnetic and paramagnetic sites, and J_{ex}^i is the (interatomic) exchange energy acting on the paramagnetic site from the ferromagnetic layers on the other side of the interface. Interatomic exchange energy has been distinguished from intra-atomic (Stoner) exchange involved in flipping the spin of a single electron. Rewriting Eq. (C9),

$$\frac{M_p^2}{\chi_v} V_{at} = 2J_{ex}^i s_f \frac{M_p}{2\mu_B} V_{at}, \qquad (C11)$$

if $s_f = 1/2$, appropriate for $4\pi M_s \sim 10$ kG,

$$J_{ex}^i = 2\mu_B \frac{M_p}{\chi_v}, \qquad (C12)$$

and substituting for χ_v through Eq. (C4),

$$J_{ex}^i = \frac{M_p}{\mu_B N_0 S}. \qquad (C13)$$

In the XMCD experiment, we measure the thickness-averaged magnetization as $\langle M \rangle$ in an [F/N]$_n$ superlattice. We make a simplifying assumption that the exchange acts only on nearest neighbors and so only the near-interface atomic layer has a substantial magnetization. We can then estimate M_p from $\langle M \rangle$ through

$$\langle M \rangle t_p = 2M_p t_i, \qquad (C14)$$

where t_i is the polarized interface-layer thickness of N [36]. Since the interface exists on both sides of the N layer, $2t_i$ is the thickness in contact with F. Finally,

$$J_{ex} = \frac{1}{2}\frac{\langle M \rangle}{\mu_B N_0 S}\frac{t_p}{t_i}. \qquad (C15)$$

The exchange energy acting on each interface atom, from all neighbors, is $J_{ex}^{\text{Pt}} = 109$ meV for Pt and $J_{ex}^{\text{Pd}} = 42$ meV for Pd. Per nearest neighbor for an ideal F/N(111) interface, it is $J^{\text{Py}|\text{Pt}} = 36$ meV and $J^{\text{Py}|\text{Pd}} = 14$ meV. Per nearest neighbor for an intermixed interface (6 nn), the values drop to 18 meV and 7 meV, respectively.

Since explicit calculations for these systems are not in the literature, we can compare indirectly with theoretical values. Dennler [41] showed that at a $(3d)$F/$(4d)$N interface (e.g., Co/Rh), there is a geometrical enhancement in the moment induced in N per nearest neighbor of F. The $4d$ N atoms near the F interface have larger induced magnetic moments per nearest neighbor of F by a factor of four. Specific calculations exist of $J^{\text{F}|\text{N}}$ (per neighbor) for dilute Co impurities in Pt and dilute Fe impurities in Pd [42]. $J^{\text{Fe-Pd}} \sim 3$ meV is calculated, roughly independently of composition up to 20% Fe. If this value is scaled up by a factor of four, to be consistent

with the interface geometry in the XMCD experiment, it is ~ 12 meV, comparable with the value for Pd, assuming intermixing. Therefore the values calculated have the correct order of magnitude.

2. Ferromagnets

The Weiss molecular field,

$$H_W = \beta M_s, \tag{C16}$$

where β is a constant of order 10^3, can be used to give an estimate of the Curie temperature, as

$$T_C = \frac{\mu_B g_J J(J+1)}{3k_B} H_W. \tag{C17}$$

Density functional theory calculations have been used to estimate the molecular field recently [42,43]; for spin type, the $J(J+1)$ term is substituted with $\langle s \rangle^2$, giving an estimate of

$$T_C = \frac{2\langle s \rangle^2 J_0}{3k_B}, \tag{C18}$$

where $\langle s \rangle$ is the number of spins on the atom as in Eq. (C10); see the text by Stöhr and Siegmann [44]. $\langle s \rangle$ can be estimated from $m = 1.07\,\mu_B$ for Py and $1.7\,\mu_B$ for Co, respectively. Then

$$J_0 \simeq \frac{6k_B T_C}{(m/\mu_B)^2} \tag{C19}$$

with experimental Curie temperatures of 870 and 1388 K, respectively, gives estimates of $J_0 = 293$ meV for Co and $J_0 = 393$ meV for Py.

Note that there is also a much older, simpler method. Kikuchi [45] has related the exchange energies to the Curie temperature for fcc lattices through

$$J = 0.247 k_B T_C. \tag{C20}$$

Taking 12 nearest neighbors, $12J$ gives a total energy of 222 meV for Py (870 K) and 358 meV for fcc Co (1400 K), not too far off from the DFT estimates.

Other estimates. The J_0 exchange parameter is interatomic, describing the interaction between spin clusters located on atoms. Reversing the spin of one of these clusters would change the energy J_0. The Stoner exchange Δ is different, since it is the energy involved in reversing the spin of a single electron in the electron sea. Generally Δ is understood to be greater than J_0 because it involves more Coulomb repulsion; interatomic exchange can be screened more easily by sp electrons.

This exchange energy is that which is measured by photoemission and inverse photoemission. Measurements are quite different for Py and Co. Himpsel [40] finds an exchange splitting of $\Delta = 270$ meV for Py, which is not too far away from the Weiss J_0 value. For Co, however, the value is between 0.9 and 1.2 eV, different by a factor of four. For Co the splitting needs to be estimated by a combination of photoemission and inverse photoemission because the splitting straddles E_F [46].

For comparison with the paramagnetic values of J_{ex}^i, we use the J_0 estimates, since they both involve a balance between Zeeman energy (here in the Weiss field) and Heisenberg interatomic exchange. Nevertheless the exchange splitting Δ_{ex} is more relevant for the estimate of $\lambda_c = h v_g/(2\Delta_{ex})$. For Py, the predicted value of λ_c from the photoemission value (through $\lambda_c = \pi/|k^\uparrow - k^\downarrow|$) is 1.9 nm, not far from the experimental value of 1.2 nm.

---

[1] W. Weber, S. Riesen, and H. Siegmann, Science **291**, 1015 (2001).

[2] M. D. Stiles and A. Zangwill, Phys. Rev. B **66**, 014407 (2002).

[3] E. Saitoh, M. Ueda, H. Miyajima, and G. Tatara, Appl. Phys. Lett. **88**, 182509 (2006).

[4] I. M. Miron, K. Garello, G. Gaudin, P.-J. Zermatten, M. V. Costache, S. Auffret, S. Bandiera, B. Rodmacq, A. Schuhl, and P. Gambardella, Nature (London) **476**, 189 (2011).

[5] L. Liu, T. Moriyama, D. C. Ralph, and R. A. Buhrman, Phys. Rev. Lett. **106**, 036601 (2011).

[6] Z. Feng, J. Hu, L. Sun, B. You, D. Wu, J. Du, W. Zhang, A. Hu, Y. Yang, D. M. Tang *et al.*, Phys. Rev. B **85**, 214423 (2012).

[7] H. Nakayama, K. Ando, K. Harii, T. Yoshino, R. Takahashi, Y. Kajiwara, K. Uchida, Y. Fujikawa, and E. Saitoh, Phys. Rev. B **85**, 144408 (2012).

[8] K.-S. Ryu, L. Thomas, S.-H. Yang, and S. Parkin, Nat. Nanotechnol. **8**, 527 (2013).

[9] J.-C. Rojas-Sánchez, N. Reyren, P. Laczkowski, W. Savero, J.-P. Attané, C. Deranlot, M. Jamet, J.-M. George, L. Vila, and H. Jaffrès, Phys. Rev. Lett. **112**, 106602 (2014).

[10] Q. Zhang, S.-i. Hikino, and S. Yunoki, Appl. Phys. Lett. **99**, 172105 (2011).

[11] W. Zhang, W. Han, X. Jiang, S.-H. Yang, and S. S. P. Parkin, Nat. Phys. **11**, 496 (2015).

[12] M. Tokaç, S. A. Bunyaev, G. N. Kakazei, D. S. Schmool, D. Atkinson, and A. T. Hindmarch, Phys. Rev. Lett. **115**, 056601 (2015).

[13] A. Ghosh, J. F. Sierra, S. Auffret, U. Ebels, and W. E. Bailey, Appl. Phys. Lett. **98**, 052508 (2011).

[14] A. Ghosh, S. Auffret, U. Ebels, and W. E. Bailey, Phys. Rev. Lett. **109**, 127202 (2012).

[15] Y. Niimi, D. Wei, H. Idzuchi, T. Wakamura, T. Kato, and Y. C. Otani, Phys. Rev. Lett. **110**, 016805 (2013).

[16] C. T. Boone, J. M. Shaw, H. T. Nembach, and T. J. Silva, J. Appl. Phys. **117**, 223910 (2015).

[17] T. Nan, S. Emori, C. T. Boone, X. Wang, T. M. Oxholm, J. G. Jones, B. M. Howe, G. J. Brown, and N. X. Sun, Phys. Rev. B **91**, 214416 (2015).

[18] A. Ruiz-Calaforra, T. Brächer, V. Lauer, P. Pirro, B. Heinz, M. Geilen, A. V. Chumak, A. Conca, B. Leven, and B. Hillebrands, J. Appl. Phys. **117**, 163901 (2015).

[19] Y. Tserkovnyak, A. Brataas, and G. E. W. Bauer, Phys. Rev. Lett. **88**, 117601 (2002).

[20] J. Foros, G. Woltersdorf, B. Heinrich, and A. Brataas, J. Appl. Phys. **97**, 10A714 (2005).

[21] J.-S. Lee, J.-Y. Kim, J. H. Shim, B. I. Min, K.-B. Lee, and J.-H. Park, Phys. Rev. B **76**, 060403 (2007).

[22] W. E. Bailey, A. Ghosh, S. Auffret, E. Gautier, U. Ebels, F. Wilhelm, and A. Rogalev, Phys. Rev. B **86**, 144403 (2012).

[23] F. Wilhelm, P. Poulopoulos, G. Ceballos, H. Wende, K. Baberschke, P. Srivastava, D. Benea, H. Ebert, M. Angelakeris, N. K. Flevaris *et al.*, Phys. Rev. Lett. **85**, 413 (2000).

[24] J. Vogel, A. Fontaine, V. Cros, F. Petroff, J.-P. Kappler, G. Krill, A. Rogalev, and J. Goulon, Phys. Rev. B **55**, 3663 (1997).

[25] W. Zhang, M. B. Jungfleisch, W. Jiang, Y. Liu, J. E. Pearson, S. G. E. te Velthuis, A. Hoffmann, F. Freimuth, and Y. Mokrousov, Phys. Rev. B **91**, 115316 (2015).

[26] Y. Tserkovnyak and A. Brataas, Rev. Mod. Phys. **77**, 1375 (2005).

[27] A. Brataas, Yu. V. Nazarov, and G. E. W. Bauer, Phys. Rev. Lett. **84**, 2481 (2000).

[28] M. Zwierzycki, Y. Tserkovnyak, P. J. Kelly, A. Brataas, and G. E. W. Bauer, Phys. Rev. B **71**, 064420 (2005).

[29] Y. Liu, Z. Yuan, R. J. H. Wesselink, A. A. Starikov, and P. J. Kelly, Phys. Rev. Lett. **113**, 207202 (2014).

[30] K. Chen and S. Zhang, Phys. Rev. Lett. **114**, 126602 (2015).

[31] Y. Sun, H. Chang, M. Kabatek, Y.-Y. Song, Z. Wang, M. Jantz, W. Schneider, M. Wu, E. Montoya, B. Kardasz *et al.*, Phys. Rev. Lett. **111**, 106601 (2013).

[32] C. T. Boone, H. T. Nembach, J. M. Shaw, and T. J. Silva, J. Appl. Phys. **113**, 153906 (2013).

[33] L. Liu, C.-F. Pai, Y. Li, H. W. Tseng, D. C. Ralph, and R. A. Buhrman, Science **336**, 555 (2012).

[34] J. Kohlhepp, G. Strijkers, H. Wieldraaijer, and W. J. M. de Jonge, Phys. Status Solidi A **189**, 701 (2002).

[35] A. Rogalev and F. Wilhelm, Phys. Met. Metallogr. **116**, 1285 (2015).

[36] The values of interface moment M_i in Pt and Pd are calculated confining the volume-averaged moment to the first 2 atomic planes at both the Py|N|Py interfaces of the stack. Given the bulk (111)-plane distance $a/\sqrt{3}$ (with a as in Table I), the polarized-interface-layer thickness $t_i = 2(a/\sqrt{3})$ is therefore defined. Considering the decay of the moment with distance from the interface, t_i would capture about 70% of the total induced moment [23,24].

[37] S. Misawa and K. Kanematsu, *3d, 4d, and 5d Elements, Alloys, and Compounds* (Springer Materials, Springer-Verlag, Berlin, Heidelberg, 1986), Vol. 19a, Chap. 1.3.1.

[38] H. Song, L. Cheng, and W. Bailey, J. Appl. Phys. **95**, 6592 (2004).

[39] D. H. Dye, J. B. Ketterson, and G. W. Crabtree, J. Low Temp. Phys. **30**, 813 (1978).

[40] D. Y. Petrovykh, K. N. Altmann, H. Höchst, M. Laubscher, S. Maat, G. J. Mankey, and F. J. Himpsel, Appl. Phys. Lett. **73**, 3459 (1998).

[41] S. Dennler, J. Hafner, M. Marsman, and J. Morillo, Phys. Rev. B **71**, 094433 (2005).

[42] S. Polesya, S. Mankovsky, O. Sipr, W. Meindl, C. Strunk, and H. Ebert, Phys. Rev. B **82**, 214409 (2010).

[43] M. Pajda, J. Kudrnovský, I. Turek, V. Drchal, and P. Bruno, Phys. Rev. B **64**, 174402 (2001).

[44] J. Stöhr and H. C. Siegmann, *Magnetism: From Fundamentals to Nanoscale Dynamics* (Springer-Verlag, Berlin, Heidelberg, 2006).

[45] R. Kikuchi, Ann. Phys. **4**, 1 (1958).

[46] C. M. Schneider, P. Bressler, P. Schuster, J. Kirschner, J. J. de Miguel, and R. Miranda, Phys. Rev. Lett. **64**, 1059 (1990).